ELSEVIER

Biophysical Chemistry 113 (2005) 223–232

Biophysical Chemistry

www.elsevier.com/locate/bpc

Structure and properties of phospholipid–peptide monolayers containing monomeric SP-$B_{1–25}$ I. Phases and morphology by epifluorescence microscopy

Nilanjana Biswas[a], Saratchandra Shanmukh[a], Alan J. Waring[b,c], Frans Walther[c], Zhendong Wang[d], Y. Chang[d], Robert H. Notter[d], Richard A. Dluhy[a,*]

[a]*Department of Chemistry, University of Georgia, Athens, GA 30602-2556, USA*
[b]*Division of Infectious Diseases, Center for the Health Sciences, Department of Medicine, UCLA, 10833 Le Conte Avenue, Los Angeles, CA 90095, USA*
[c]*Department of Pediatrics, Research and Education Institute at Harbor-UCLA Medical Center, 1124 West Carson Street, Building F-5 South, Torrance, CA 90502, USA*
[d]*University of Rochester, Department of Pediatrics, Box 850, Neonatology, 601 Elmwood Avenue, Rochester, NY 14642, USA*

Received 20 July 2004; received in revised form 15 September 2004; accepted 15 September 2004
Available online 18 October 2004

Abstract

Epifluorescence microscopy was used to study the structure and phase behavior of phospholipid films containing a human-sequence monomeric SP-$B_{1–25}$ synthetic peptide (mSP-$B_{1–25}$). Measurements were done directly at the air–water (A/W) interface on films in a Langmuir–Whilhelmy balance coupled to a fluorescence microscope and real-time detection system to yield an approximate optical resolution of 1 μm. Fluorescence was achieved by laser excitation of 2-(4,4-difluoro-5,7-dimethyl-4-bora-3a,4a-diaza-*s*-indacene-3-dodecanoyl)-1-hexadecanoyl-*sn*-glycero-3-PC (BODIPY-PC, concentration ≤1 mol%). The presence of mSP-$B_{1–25}$ in films of 4:1 (mol/mol) 1,2-dipalmitoyl-*sn*-glycero-3-phosphocholine (DPPC)/1,2-dioleoyl-*sn*-glycero-3-[phospho-*rac*-(1-glycerol)] (sodium salt) (DOPG) had a substantial effect on lipid morphology and phase behavior that depended on both surface pressure and peptide concentration (10, 5, and 1 wt.%). The mSP-$B_{1–25}$ peptide tended to fluidize phospholipid monolayers based on expanded molecular areas and reduced collapse pressures. In addition, epifluorescence measurements revealed the formation of solid-phase domains apparent as three-armed counter-clockwise spirals separated from regions of fluid liquid-expanded phase domains in compressed phospholipid–peptide films. The appearance of these separated solid-phase domains resembled pure *L*-DPPC rather than the ensemble-type solid domains found in films of DPPC/DOPG alone and were most apparent when 10 wt.% mSP-$B_{1–25}$ was present. In contrast, films containing lower, more physiological mSP-$B_{1–25}$ contents of 5 and 1 wt.% exhibited a prominent intermediate 'dendritic' phase that increased in extent as surface pressure was raised. This phase was characterized by branching structures that formed a lattice-like mesh network with fluorescence intensities between a dye-depleted solid domain and a dye-enriched liquid phase. These results indicate that mSP-$B_{1–25}$ at near-physiological levels produces morphological changes in phospholipid monolayers analogous to those observed for native SP-$B_{1–79}$.

Keywords: mSP-$B_{1–25}$; Epifluorescence microscopy; Air–water interface; Lung surfactants; Surfactant protein (SP)-B; Synthetic peptides

Abbreviations: ALI, acute lung injury; ARDS, acute respiratory distress syndrome; A/W, air–water; BODIPY-PC, 2-(4,4-difluoro-5,7-dimethyl-4-bora-3a,4a-diaza-*s*-indacene-3-dodecanoyl)-1-hexadecanoyl-*sn*-glycero-3-phosphocholine; DPPC, 1,2-dipalmitoyl-*sn*-glycero-3-phosphocholine; DOPG, 1,2-dioleoyl-*sn*-glycero-3-[phospho-*rac*-(1-glycerol)] (sodium salt); HEPES, *N*-(2-hydroxyethyl)piperizine-*N*′-(2-ethanesulfonic acid); HMP, 4-hydroxymethylphenoxyacetyl-4′-methylbenzyhydrylamine resin; RDS, respiratory distress syndrome; SP-B/C, mixture of hydrophobic surfactant peptides B and C; SP-B, pulmonary surfactant protein B; SP-$B_{1–25}$, synthetic peptide containing the first 25 amino acids of the N-terminus of SP-B; SP-C, pulmonary surfactant protein C; TFA, trifluoroacetic acid; TFE, trifluoroethanol.

* Corresponding author. Tel.: +1 706 542 1950; fax: +1 706 542 9454.

0301-4622/$ - see front matter © 2004 Elsevier B.V. All rights reserved.
doi:10.1016/j.bpc.2004.09.008

1. Introduction

Pulmonary surfactant forms a lipid–protein film that lowers and varies surface tension at the alveolar air–water (A/W) interface in the mammalian lungs. One of the most important components of this film is surfactant protein B (SP-B). SP-B is a small (MW~8700 Da), lipid-associating protein that belongs to the Saposin superfamily that includes Saposin B, Saposin C, granulysin, and NK-lysin. These proteins share a common disulfide connectivity that constrains their overall backbone to form an amphipathic helix hairpin structure [1], which has been conserved in SP-B for an estimated 300 million years [2]. The mature SP-B protein exists not only as a monomer, but also as oligomers, such as a covalently linked homodimer that is prevalent in humans. The presence of endogenous SP-B is crucial for normal lung function, since gene knockouts for this protein are lethal in mice [3] and hereditary SP-B deficiency is fatal in humans [4]. In addition, organic solvent extracts of animal lung surfactant that contain SP-B are the basis for highly active exogenous lung surfactants used to treat premature infants with the respiratory distress syndrome (RDS) as well as patients with clinical acute lung injury (ALI) or the acute respiratory distress syndrome (ARDS) [5,6].

Although lung surfactant extracts containing SP-B are effective in treating RDS, less is known about the specific molecular mechanisms of action of this protein directly within lipid–protein monolayers. The full-length SP-B protein has multiple distinct domains, e.g., Refs. [7,8]. The N-terminal domain has a short insertion sequence that can assume an extended β-sheet conformation and is adjacent to a stable amphipathic helix. This is followed by a short hydrophobic sequence encompassing residues 26–34, which contain alanine–valine repeats having some α-helical/β-sheet conformational flexibility [8] terminated by a disulfide-stabilized bend region [9]. The bend domain is next to a surface helical sequence that allows disulfide connectivity to form the homodimer. These mid-protein sequences are followed by a short amphipathic leucine repeat that also can display α-helix/β-sheet conformational interconversion [10]. This sequence has served as a template for the synthetic KL4 peptide used in exogenous surfactant replacement applications [11]. Finally, recent structural NMR studies of the C-terminal domain of SP-B have shown that it can assume an amphipathic helical conformation in structure-promoting solvents and in micelles [12], suggesting that this domain optimizes interactions with surfactant lipids much like the N-terminal segment of the protein.

The distribution of cationic residues like lysine and arginine largely within the N- and C-terminal amphipathic helical segments of SP-B is functionally relevant, since these residues are important for interacting with anionic lipids [13,14]. This, along with the stable amphipathic helical structure of the N-terminal region, makes it particularly interesting for structural and functional investigations. A number of studies have investigated the biophysical actions of monomer and dimer human-sequence peptides incorporating the 25 amino acids at the N-terminus of SP-B (SP-$B_{1–25}$). SP-$B_{1–25}$ monomer or dimer peptides emulate a number of the biophysical actions of full-length SP-B, including associating with surfactant lipids [13,15], promoting lipid mixing between vesicles [16], and participating in surface pressure-dependent domain formation and buckling in lipid films [14,17–19]. Also, antibodies developed against SP-$B_{1–25}$ have been found to interact with the native full-length protein [15]. In addition, synthetic surfactants containing lipids combined with SP-$B_{1–25}$ have significant physiological activity in mitigating surfactant deficiency and/or dysfunction in animal models [20–22]. Although several experimental and computer investigations of the conformation of SP-$B_{1–25}$ have been done [23–26], there is little information on its properties in surface films containing the major lung surfactant phospholipid dipalmitoyl phosphatidylcholine (1,2-dipalmitoyl-*sn*-glycero-3-phosphocholine, DPPC) plus a physiologically relevant anionic lipid like dioleoyl phosphatidylglycerol (1,2-dioleoyl-*sn*-glycero-3-[phospho-*rac*-(1-glycerol)] (sodium salt), DOPG). The present study examines in detail the molecular biophysical behavior of monomeric SP-$B_{1–25}$ (mSP-$B_{1–25}$) directly in spread films with 4:1 DPPC/DOPG at the air–water (A/W) interface. Emphasis in this paper is on the effects of mSP-$B_{1–25}$ on film domain and phase behavior by epifluorescence, while a companion paper examines the molecular interactions and interfacial orientation of the peptide in the film by polarization modulation–infrared reflectance-absorption spectroscopy.

2. Materials and Methods

2.1. Synthetic materials

The synthetic phospholipids 1,2-dipalmitoyl-*sn*-glycero-3-phosphocholine (DPPC) and 1,2-dioleoyl-*sn*-glycero-3-[phospho-*rac*-(1-glycerol)] (sodium salt) (DOPG) were purchased from Avanti Polar Lipids (Alabaster, AL). These lipids were specified as >99% pure and were used as supplied. An acyl chain-labeled fluorescent lipid probe (2-(4,4-difluoro-5,7-dimethyl-4-bora-3a,4a-diaza-*s*-indacene-3-dodecanoyl)-1-hexadecanoyl-*sn*-glycero-3-PC, BODIPY-PC) was obtained from Molecular Probes (Eugene, OR). ACS grade NaCl and high-performance liquid chromatography (HPLC) grade methanol and chloroform were obtained from J.T. Baker (Phillipsburg, NJ). Ultrapure H_2O used to form film subphases and in all cleaning procedures was obtained from a Barnstead (Dubuque, IA) ROpure/Nanopure reverse osmosis/deionization system and had a nominal resistivity of 18.3 MΩ cm. Film subphases in all experiments were 120 mM NaCl adjusted to pH 7 with a phosphate buffer.

2.2. Peptide synthesis and purification

SP-$B_{1–25}$ (NH_2–FPIPLPYCWLCRALIKRIQAMIPKG–COOH) was made by solid-phase peptide synthesis employing *O*-fluorenylmethyl-oxycarbonyl (Fmoc) chemistry. Fmoc amino acids and coupling agents were from AnaSpec (San Jose, CA). Solvents and other reagents used for peptide synthesis and purification were HPLC grade or better (Fisher Scientific, Tustin, CA; Aldrich Chemical, Milwaukee, WI). The peptide was synthesized on a 0.25-mmol scale with an ABI 431A peptide synthesizer configured for FastMoc™ double coupling cycles [27]. The peptide was synthesized with a pre-derivatized *N*-α-Fmoc-glycine 4-hydroxymethylphenoxyacetyl-4′ -methylbenzyhydryl-amine resin (HMP) resin (AnaSpec). Deprotection and cleavage of the peptide from the resin was carried out using trifluoroacetic acid (TFA)/thioanisol/EDT/phenol/water (10:0.5:0.25:0.5:0.5 by vol.) for 2 h followed by precipitation cold with *t*-butyl ether. The crude product was then purified by preparative reverse-phase HPLC with a Vydac C-18 column, using a water/acetonitrile linear gradient with 0.1% trifluoroacetic acid as described previously [28]. The molecular weight of the peptide was determined by fast atom bombardment and/or MALDI-TOF mass spectrometry, and purity of >95% was confirmed by analytical HPLC and capillary electrophoresis.

2.3. Preparation of lipid–peptide mixtures

Stock phospholipid solutions of DPPC and DOPG (~1 mg/ml) were prepared in 3:1 $CHCl_3$/MeOH. For the lipid–peptide samples, the required volume of mSP-$B_{1–25}$ in 1:1 $CHCl_3$/MeOH was evaporated with N_2 for ~30 min to ensure complete solvent evaporation. The dried protein film was then dissolved in a volume of 2,2,2-trifluoroethanol (TFE), and an appropriate volume of DPPC/DOPG stock solution was added to the protein solution in TFE. The resultant phospholipid–protein solution was evaporated for ~45 min with N_2 and then left overnight in a vacuum desiccator for complete elimination of solvent. The dried phospholipid–protein sample was then redissolved in 3:1 $CHCl_3$/MeOH, and 1 mol% of BODIPY-PC dye was added to the final solution for fluorescence studies.

2.4. Epifluorescence and surface balance methods

The epifluorescence imaging microscope used in this work was built around a commercial epifluorescence microscope body (AxioTech Vario, Carl Zeiss, Jena, Germany). Sample illumination was accomplished using a 100-W Hg lamp. Fluorescence imaging measurements utilized a BODIPY-PC fluorescent lipid probe that was added to the lipid–peptide mixtures at a concentration of 1 mol% or less. Fluorescence was excited in the BODIPY probe using the Hg lamp and observed using the Zeiss microscope equipped with the Zeiss standard filter set #09. This optical filter set uses a 450–490-nm excitation bandpass filter, a 510-nm beamsplitter, and a 515-nm long-pass emission filter. Real-time fluorescence detection utilized a low-light-level camera (SIT camera C2400-08, Hamamatsu, Japan). Images were directly stored into computer memory via an on-line image processor (Argus 20, Hamamatsu, Japan). The digital resolution of the images was better than 3 pixels/μm, resulting in an optical resolution of approximately 1 μm. A custom-designed Langmuir–Wilhelmy film balance (Nima, Coventry, England) interfaced to the microscope was used to study film behavior as a function of surface area at room temperature (22.0±0.3 °C). The trough of the film balance measured 60×8 cm, and surface pressure was monitored during compression with a pressure sensor utilizing a filter paper Wilhelmy plate. Isotherms were generally measured with a film compression ratio (initial area to final area) of 5.6, resulting in a compression rate of 88 min/compression or 0.82 $Å^2$/molecule/min for the pure DPPC/DOPG lipid mixture. The film balance was placed on a computer-controlled *x*–*y* stage (Aerotech, Pittsburgh, PA) in order to adjust the observation area and to compensate for any small film drift. The entire microscope and film balance assembly was isolated from building vibrations by an active vibration isolation table (Halcyon, Switzerland).

3. Results and discussion

3.1. Isotherms

Fig. 1 shows a representative surface pressure–area (*π*–*A*) isotherm obtained for a 4:1 (mol/mol) DPPC/DOPG monomolecular film. The presence of the unsaturated C18:1 acyl chains of DOPG in the mixed lipid film resulted in a compression isotherm that lacked a distinctive plateau

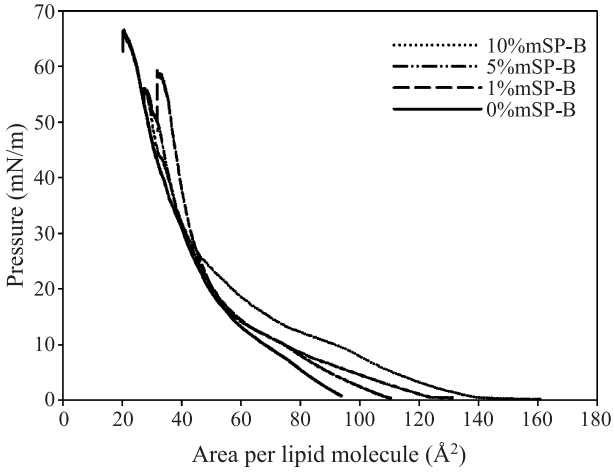

Fig. 1. Pressure–area isotherms (*T*=22.0±0.3 °C) of surface monolayers of 4:1 (mol/mol) DPPC/DOPG. Film subphases contained 120 mM NaCl buffered to pH 7. Concentrations of mSP-$B_{1–25}$ in the spread interfacial film were 10, 5, 1, or 0 wt.% (lipids alone).

region characteristic of a first-order transition, consistent with previous findings [29]. Isotherms for films of the same lipids but containing differing amounts of mSP-$B_{1–25}$ (10, 5, and 1 wt.%) are also included in Fig. 1. The addition of mSP-$B_{1–25}$ was found to result in an increase in molecular area and a shift in transition pressure with increasing peptide content at surface pressures less than ~30 mN/m. At surface pressures above ~30 mN/m, the largest expansion in molecular area relative to the pure lipids was found in films containing 1 wt.% of mSP-$B_{1–25}$ peptide. In all the lipid–peptide films, collapse surface pressures were lower than that of a binary monolayer of 4:1 DPPC/DOPG alone. These π–A isotherm changes are indicative of a fluidizing effect from the presence of the mSP-$B_{1–25}$ peptide in the phospholipid film. A fluidizing effect on the solid phase of lipid films has previously been observed for mixed natural surfactant proteins SP-B/C [30] and fluorescently labeled pulmonary surfactant proteins B and C (SP-B and SP-C) [31–33]. A fluidizing effect has also been reported for mSP-$B_{1–25}$ in palmitic acid monolayers [14].

In terms of physiological relevance, surface pressure–area isotherms and film phase behavior were assessed here at room temperature (22 °C) rather than body temperature (37 °C); However, major changes in film morphology or phase behavior would not be expected to occur between 22 and 37 °C in the films studied based on the gel-to-liquid crystal transition temperatures of the phospholipid components. DPPC (T_c=41 °C) is in the rigid gel phase at both room and body temperature, while DOPC (T_c=−18 to −22 °C) is in the liquid crystal phase at both temperatures. Whole lung surfactant contains a variety of phospholipids in addition to DPPC and DOPC, but the majority of these phospholipid constituents also do not have gel to liquid crystal transitions between room and body temperature [5].

With regard to cycling rate effects, these surface experiments also used much slower cycling rates than those occurring at the alveolar interface during normal breathing. In this respect, the interfacial phases found in our Wilhelmy balance studies reflect quasi-static film behavior relative to the lungs in vivo. It is possible that additional surface organizational features may occur in lipid–peptide films at rapid physiological rates of compression that were not apparent at the low rates (~88 min/cycle) examined here. Nonetheless, studies of surface tension–area isotherms and molecular interactions in interfacial films on the Wilhelmy balance have proven crucial in helping to understand the functionality of various lung surfactant components (see, e.g., Refs. [34–36]), and this is also true for the present experiments.

3.2. Epifluorescence microscopy results

Fig. 2 presents fluorescence micrograph images of a lipid-only 4:1 (mol:mol) DPPC/DOPG monolayer film at the A/W interface as a function of increasing surface pressure. These images show that this particular lipid mixture develops phase-separated domain structures in a qualitatively similar fashion to that previously reported for other PC/PG mixed monolayer systems [37].

The fluorescence micrographs of a 4:1 DPPC/DOPG film containing 10 wt.% mSP-$B_{1–25}$ showed the formation of large solid-phase domains at the onset of the phase

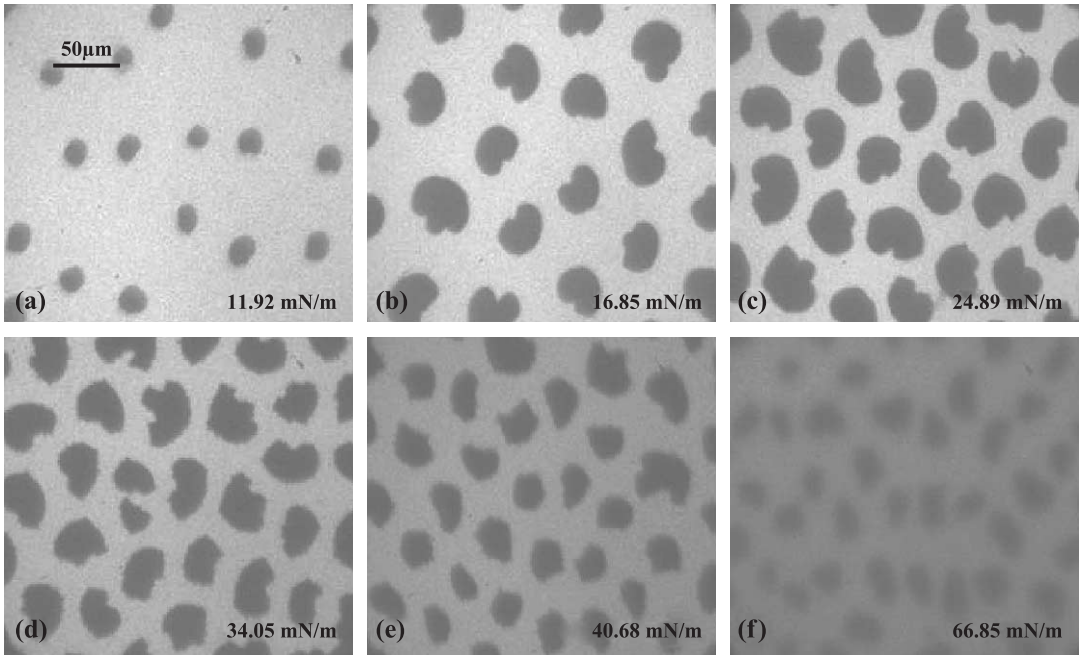

Fig. 2. Fluorescence micrographs of a monomolecular phospholipid film of 4:1 (mol/mol) DPPC/DOPG at the A/W interface. Subphase was phosphate-buffered 120 mM NaCl (pH 7, T=22.0±0.3 °C). Images are shown with increasing surface pressures as indicated. The scale bar in the upper left indicates a length of 50 μm.

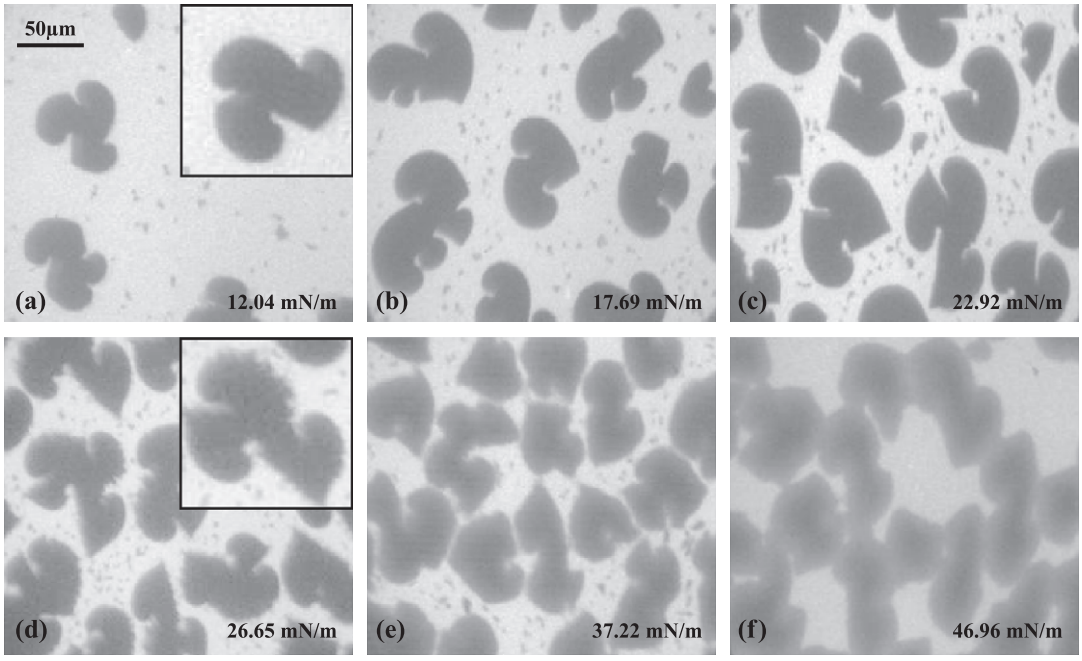

Fig. 3. Fluorescence micrographs of a monomolecular film at the A/W interface containing 4:1 (mol/mol) DPPC/DOPG with 10 wt.% mSP-$B_{1–25}$. Subphase was phosphate-buffered 120 mM NaCl (pH 7, T=22.0±0.3 °C). Images are shown with increasing surface pressures as indicated. The scale bar in the upper left indicates a length of 50 μm.

transition during monolayer compression (Fig. 3). The structures formed (e.g., Fig. 3a insert) appear as 'three-armed spirals' with the individual spiral arms curving in a counterclockwise direction, a structure that closely resembles that of the solid-phase domains of pure *L*-DPPC [38]. The fluorescence images of the peptide-containing monolayer differ substantially from those of the binary lipid mixture alone (see above), which were found to exhibit a more kidney-shaped structure at all surface pressures that was characteristic of ensemble domains [38]. The images in Fig. 3 can be inferred to be a consequence of the peptide associating most strongly with the DOPG component of the monolayer, which causes a phase separation of the less ordered (DOPG) and more ordered (DPPC) domains.

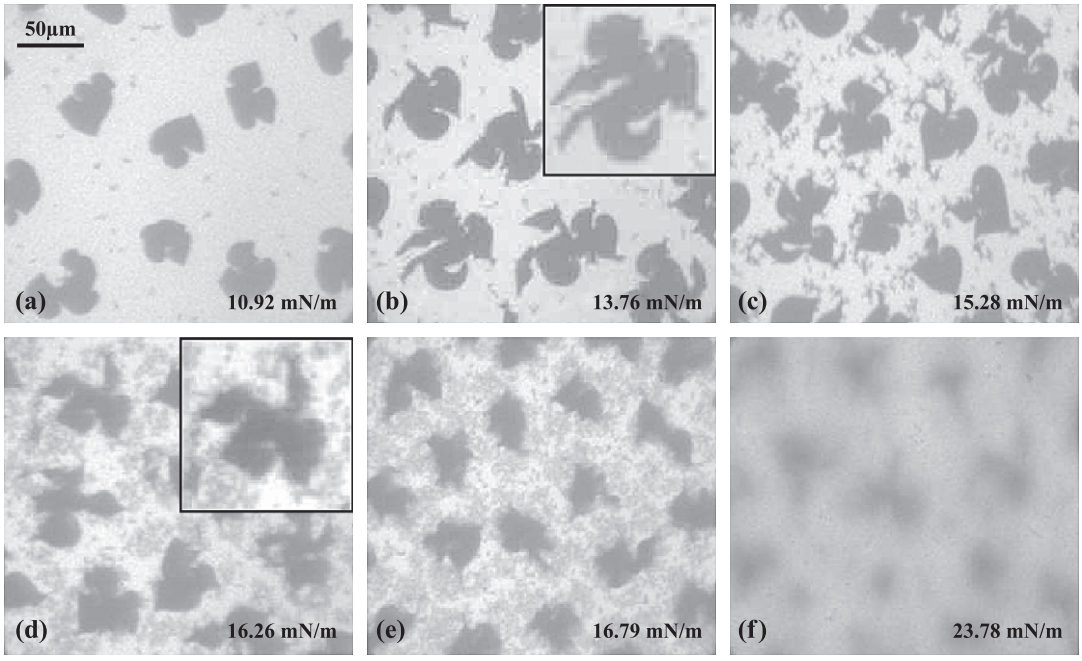

Fig. 4. Fluorescence micrographs of a monomolecular film at the A/W interface containing 4:1 (mol/mol) DPPC/DOPG with 5 wt.% mSP-$B_{1–25}$. Subphase was buffered 120 mM NaCl (pH 7, T=22.0±0.3 °C). Images are shown with increasing surface pressures as indicated. The scale bar in the upper left panel indicates a length of 50 μm.

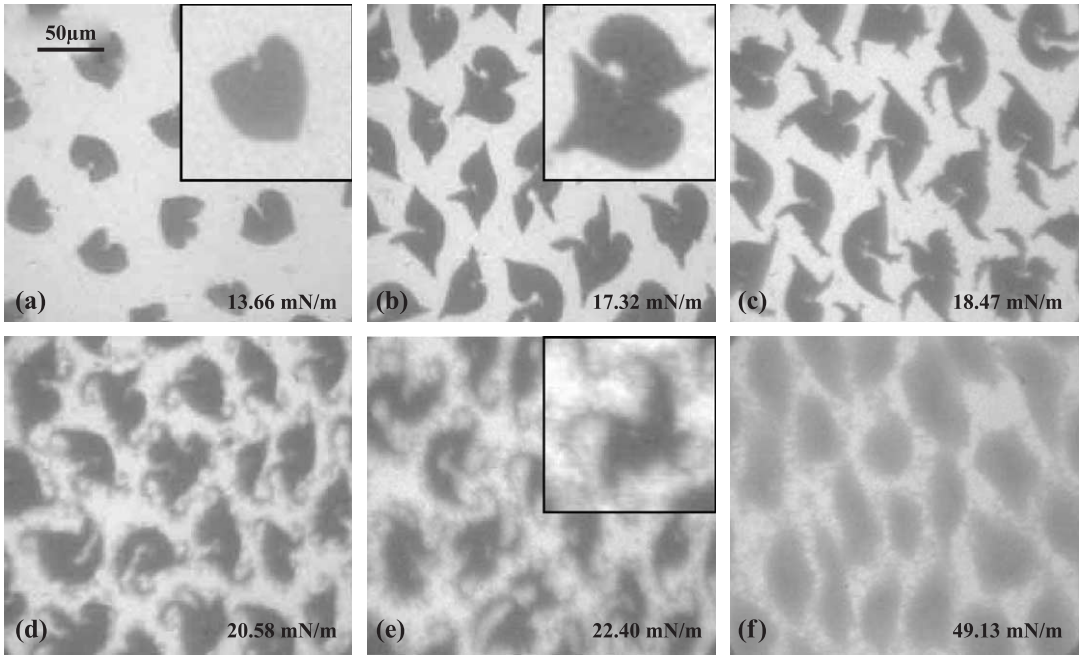

Fig. 5. Fluorescence micrographs of a monomolecular film at the A/W interface containing 4:1 (mol/mol) DPPC/DOPG with 1 wt.% mSP-$B_{1–25}$. Subphase was buffered 120 mM NaCl (pH 7, T=22.0±0.3 °C). Images are shown with increasing surface pressures as indicated. The scale bar in the upper left panel indicates a length of 50 μm.

Hence, the resulting solid lipid phase is enriched in DPPC and takes on the domain shape of pure DPPC.

This phase separation effect was prominent in films containing 10 wt.% mSP-$B_{1–25}$, but diminished as the concentration of peptide was decreased. Solid domains in 5 wt.% peptide films decreased in size as the protein content was reduced from 10 to 5 wt.% (Fig. 4) and appeared more like the condensed phase of the phospholipid mixture at the initial stages of its phase transition. Upon compression, monolayers containing 5 wt.% mSP-$B_{1–25}$ exhibited a third intermediate gray phase as the surface pressure increased (e.g., Fig. 4c–e and insert). The formation of this third phase was quite similar to that previously observed for the DPPC/DPPG system with 1 wt.% SP-B/C [30]. This intermediate

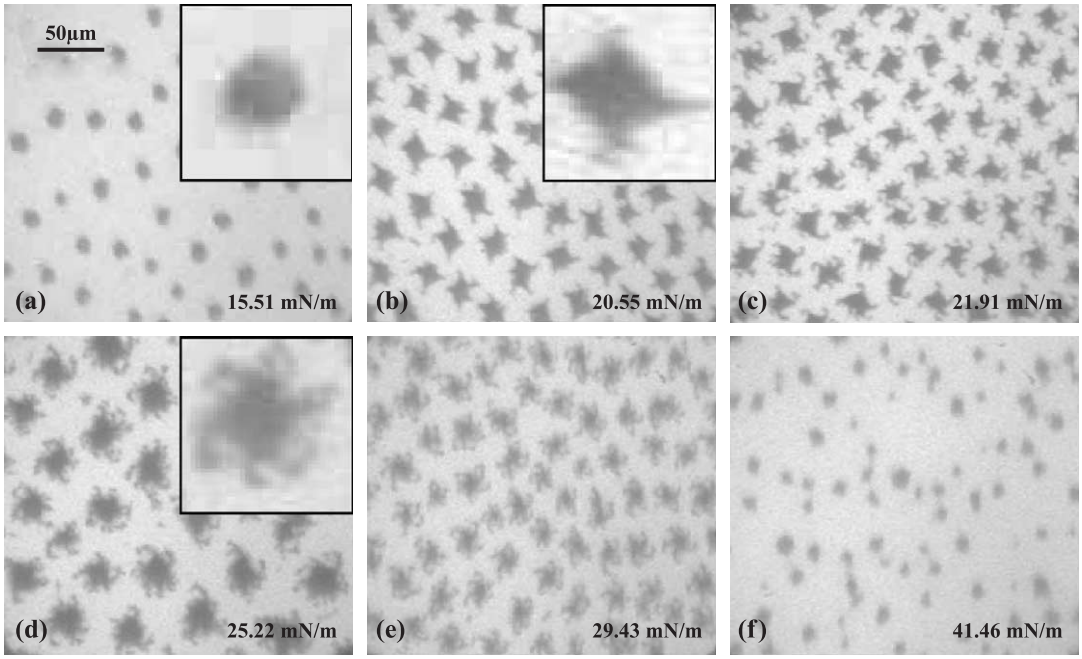

Fig. 6. Fluorescence micrographs of a monomolecular film at the A/W interface containing 4:1 (mol/mol) DPPC/DOPG with 1 wt.% mSP-$B_{1–25}$ with calcium present. Film subphase was buffered 120 mM NaCl+2 mM $CaCl_2$ (pH 7, T=22.0±0.3 °C). Images are shown with increasing surface pressures as indicated. The scale bar in the upper left panel indicates a length of 50 μm.

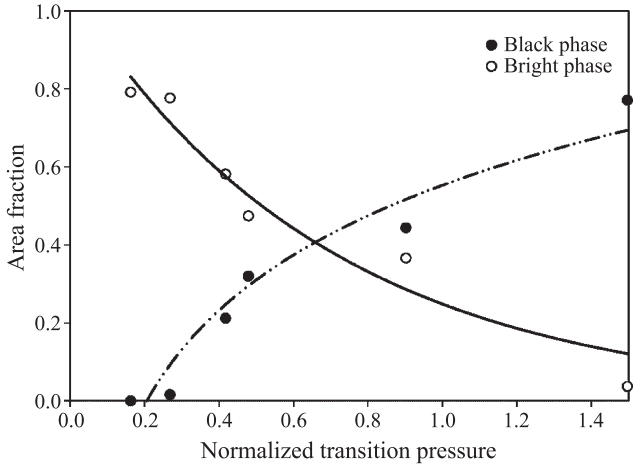

Fig. 7. Area fractions calculated from fluorescence histograms of the bright and dark phases observed in the fluorescence micrographs of the lipid-only monolayer presented in Fig. 2. Area fractions are plotted against π_n, the normalized transition pressure calculated in Eq. (1). See text.

third phase was also prominent in monolayers containing 1 wt.% mSP-$B_{1–25}$ (Fig. 5) but was much less apparent in monolayers containing 10 wt.% mSP-$B_{1–25}$ (Fig. 3).

In monolayers containing 5 and 1 wt.% of mSP-$B_{1–25}$ peptide, the intermediate phase appeared as protrusions from the compact cores of solid-phase domains into the dye-enriched liquid expanded region, giving rise to branches that had a fluorescence intensity level intermediate between that of a dye-depleted solid domain and a dye-enriched liquid region. These branches emanated outward from the solid domains resulting in the formation of a lattice-like mesh network which grew with increasing surface pressure. This mesh-like network is evident in the 5 wt.% mSP-$B_{1–25}$ images in Fig. 4c–e and in the 1 wt.% mSP-$B_{1–25}$ images in Fig. 5d–f.

Epifluorescence studies also investigated the effects of small amounts of Ca^{2+} on phospholipid–peptide monolayer morphology. The addition of 2 mM $CaCl_2$ to the subphase resulted in no major differences in the fluorescence images for the pure binary lipids or for the 10 and 5 wt.% peptide films. However, fluorescence micrographs for the monolayer containing 1 wt.% mSP-$B_{1–25}$ showed differences in the presence and absence of calcium ions (Fig. 6). In the presence of 2 mM $CaCl_2$, the solid phase grew as spherical domains at low surface pressure. These domains, however, were much smaller than in the absence of calcium (compare, for example,

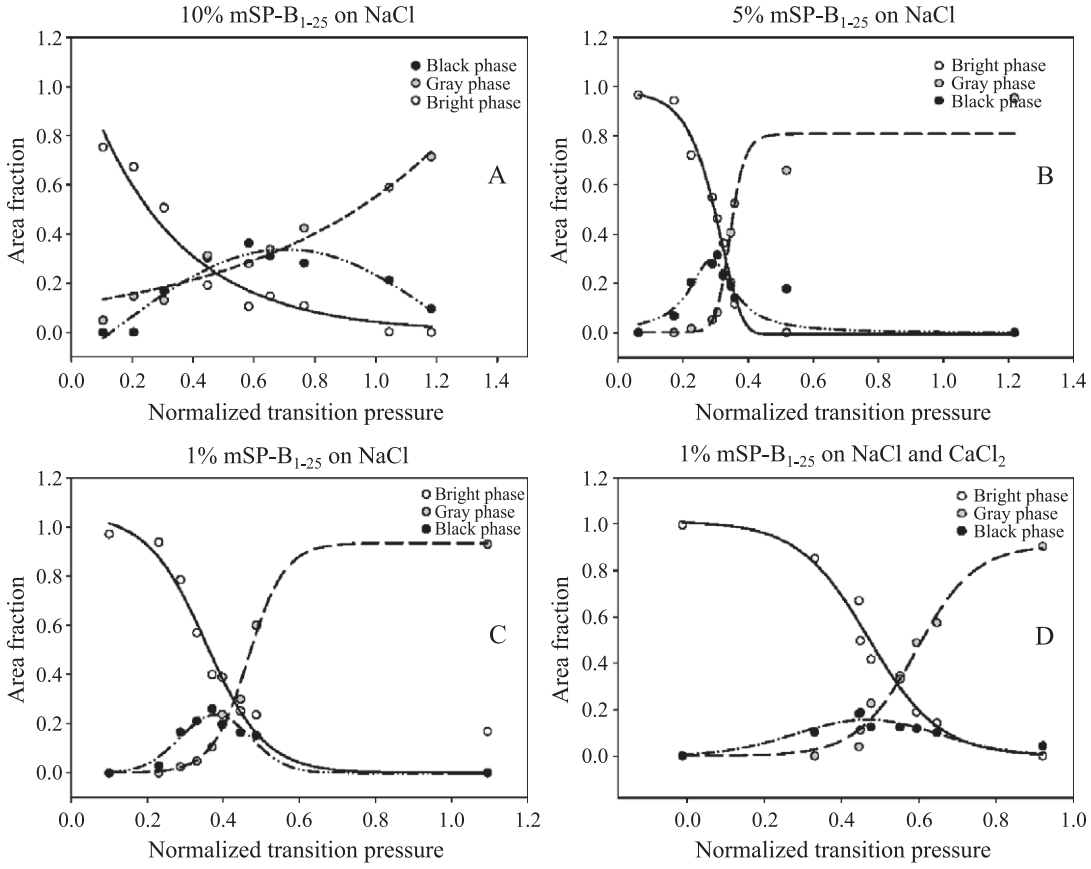

Fig. 8. Area fractions calculated from fluorescence histograms of the bright, dark and intermediate phases in the fluorescence micrographs of the monolayers containing mSP-$B_{1–25}$ presented in Figs. 3–6. Area fractions are plotted against π_n, the normalized transition pressure calculated in Eq. (1). (A) Area fractions calculated from images of 10 wt.% mSP-$B_{1–25}$ monolayer in Fig. 3. (B) Area fractions calculated from images of 5 wt.% mSP-$B_{1–25}$ monolayer in Fig. 4. (C) Area fractions calculated from images of 1 wt.% mSP-$B_{1–25}$ monolayer on NaCl subphase in Fig. 5. (D) Area fractions calculated from images of 1 wt.% mSP-$B_{1–25}$ monolayer on NaCl+$CaCl_2$ subphase in Fig. 6.

Figs. 5a and 6a). In the presence of calcium, branches of the intermediate gray phase emanated outwards from the solid domains starting at the periphery, with branches meeting at ~90° on the perimeter (Fig. 6b–e). As surface pressure increased, the number of branches also increased, with the third phase becoming dominant at small molecular areas. However, the third intermediate phase did not progress to form a lattice-like mesh structure in the 1 wt.% mSP-$B_{1–25}$ monolayer in the presence of calcium (Fig. 6).

To help quantitate the occurrence of specific phases during film compression, the distribution of fluorescence intensity levels for each image was determined as a histogram of calculated fluorescence intensity data as we have done previously for phospholipid films containing bovine SP-B/C [30]. Area fractions for a given phase were obtained from the fluorescence intensity distributions by integration over the peaks in the histograms [30]. These area fractions were then plotted in conjunction with a normalized transition pressure π_n defined as

$$\pi_n = \frac{\pi - \pi_s}{\pi_f - \pi_s} \quad (1)$$

In Eq. (1), π is the experimentally measured surface pressure, π_s is the surface pressure at the start of the transition, and π_f is the surface pressure at the end of the transition. If surface pressure–area isotherms did not allow a specific beginning and ending point for the phase transition to be defined, arbitrary values of π_s=1 mN/m and π_f=45 mN/m were utilized. Plots of area fraction vs. normalized fluorescence intensity π_n allowed the evolution of coexisting phases to be assessed as a function of the progress of the phase transition during film compression.

In order to better analyze the evolution of different monolayer phases throughout compression, the distribution of fluorescence intensity levels on recorded images was analyzed by displaying calculated histograms of fluorescence intensity as a function of normalized transition pressure π_n. Calculations of this kind are shown in Figs. 7 and 8. For the pure phospholipid mixture of 4:1 DPPC/DOPG, only two main peaks were observed in the intensity histograms, corresponding to the dark (solid) phase or the light (expanded) phase (Fig. 7). For the fluorescence images of the phospholipid–protein mixtures (Fig. 8), three peaks were observed in the intensity histograms, corresponding to the dark (solid) phase, the light (expanded) phase, and the gray (intermediate) phase shown earlier in Figs. 3–6. This latter phase exhibited a fluorescent intensity that was intermediate between the dark (solid) phase and the light (expanded) phase. By presumption, this implies an intrinsic order that is also intermediate between the fully solid and fully expanded phases. This interpretation would imply that one of the effects of mSP-$B_{1–25}$ on lipid morphology is to dissolve the solid phase and induce the formation of a new intermediate phase of reduced order. We believe that such an interpretation is warranted in the present case since the third phase only occurs upon addition of the SP-$B_{1–25}$ peptide. In addition, the increase of a third phase directly correlates with the decrease of the solid phase fraction in the monolayer. In order to study the detailed structure of the new phase, the molecular biophysics, orientation, and conformation of mSP-$B_{1–25}$ in interfacial films with 4:1 DPPC/DOPG were investigated further in a companion study using polarization modulation–infrared reflectance-absorption spectroscopy.

4. Conclusions

Surface studies investigating the biophysical roles of SP-B in films with lipids often utilize protein concentrations significantly greater than those found in native lung surfactant, e.g., Refs. [23,39–41]. The present study investigated the effects of differing surface concentrations of mSP-$B_{1–25}$ to observe the effects on film morphology and phase behavior at the A/W interface. Epifluorescence results demonstrated substantial morphological differences in phospholipid phases induced by the presence of varied concentrations of mSP-$B_{1–25}$ peptide. In general, the presence of mSP-$B_{1–25}$ had a fluidizing effect on films of 4:1 DPPC/DOPG, with increases in film molecular area and reductions in collapse pressure. These findings are in accord with previous studies suggesting that SP-B and SP-$B_{1–25}$ have a fluidizing effect on the condensed phase of lipid monolayers [14]. However, significant differences were observed in the morphology of interfacial lipid phases in compressed films containing high peptide concentrations (10 wt.% in Fig. 3 and to a lesser extent 5 wt.% in Fig. 4) compared to physiological protein contents of 1 wt.% (Fig. 5). In particular, films of 4:1 DPPC/DOPG that contained 10 wt.% peptide had a greater extent of separation into regions of solid-like and liquid-like phases during compression and had a much lower prevalence of a third phase of intermediate fluorescence intensity and presumptive molecular order. These results underscore the importance of investigating a physiologically relevant range of surfactant peptide contents in biophysical studies.

The third phase introduced by the presence of mSP-$B_{1–25}$ in mixed monolayers with 4:1 DPPC/DOPG was demonstrable by fluorescence microscopy but could not be recognized simply from the surface pressure–area isotherms of the compressed film. This phase appeared gray on epifluorescent imaging and was morphologically distinct from the dye-enriched liquid expanded phase (which was bright in appearance) and the dye-depleted solid condensed phase (which was dark in appearance). This intermediate fluorescence intensity phase is apparently formed as the result of peptide-mediated dissolution of solid phase film material. Plots portraying the variation of the area fraction with the reduced transition pressure (from the analysis of the fluorescence intensity histograms) provided a graphical representation of this effect. The growth patterns found for the intermediate phase in the

present epifluorescence studies were quite similar (although not identical) to those observed in 7:1 (mol/mol) DPPC/DPPG films containing 1 wt.% of purified bovine SP-B/C [30]. Therefore, the origin of this new phase can be attributed to some extent to the presence of SP-B-related interactions common between the two systems. The N-terminal 1–25 segment of the monomer SP-B protein is one component of the 'intermediate phase' and most likely interacts electrostatically with the anionic PG head group. In addition, peptide interactions with the zwitterionic head group of DPPC may also be involved in generating the intermediate phase. Further studies are needed to define more precisely the composition and specific molecular mechanisms of formation of this interfacial phase induced in phospholipid monolayers by mSP-$B_{1–25}$.

Acknowledgements

The financial support of the US Public Health Service through National Institutes of Health grants EB001956 (R.A.D.), HL56176 (R.H.N.), and HL55534 (F.J.W. and A.J.W.) is gratefully acknowledged.

References

[1] R.S. Munford, P.O. Sheppard, P.J. O'Hara, Saposin-like proteins (SAPLIP) carry out diverse functions on a common backbone structure, J. Lipid Res. 36 (1995) 1653–1663.
[2] J.H. Power, I.R. Doyle, K. Davidson, T.E. Nicholas, Ultrastructural and protein analysis of surfactant in the Australian lungfish *Neoceratodus forsteri*: evidence for conservation of composition for 300 million years, J. Exp. Biol. 202 (1999) 2543–2550.
[3] J.C. Clark, S.E. Wert, C.J. Bachurski, M.T. Stahlman, B.R. Stripp, T.E. Weaver, J.A. Whitsett, Targeted disruption of the surfactant protein B gene disrupts surfactant homeostasis, causing respiratory failure in newborn mice, Proc. Natl. Acad. Sci. U. S. A. 92 (1995) 7794–7798.
[4] L.M. Nogee, G. Garnier, H.C. Dietz, L. Singer, A.M. Murphy, D.E. deMello, H.R. Colten, A mutation in the surfactant protein B gene responsible for fatal neonatal respiratory disease in multiple kindreds, J. Clin. Invest. 93 (1994) 1860–1863.
[5] R.H. Notter, Lung Surfactants: Basic Science and Clinical Applications, Marcel Dekker, New York, 2000.
[6] P. Chess, J.N. Finkelstein, B.A. Holm, R.H. Notter, Surfactant Replacement Therapy in Lung Injury, in: R.H. Notter, J.N. Finkelstein, B.A. Holm (Eds.), Lung Injury: Mechanisms, Pathophysiology and Therapy, Marcel Dekker, New York, 2005, (in press).
[7] S. Zaltash, M. Palmblad, T. Curstedt, J. Johansson, B. Persson, Pulmonary surfactant protein B: a structural model and a functional analogue, Biochim. Biophys. Acta 1466 (2000) 179–186.
[8] C.R. Flach, P. Cai, D. Dieudonne, J.W. Brauner, K.M.W. Keough, J. Stewart, R. Mendelsohn, Location of structural transitions in an isotopically labeled lung surfactant SP-B peptide by IRRAS, Biophys. J. 85 (2003) 340–349.
[9] A.J. Waring, K.F. Faull, C. Leung, A. Chang-Chien, P. Mercado, H.W. Taeusch, L.M. Gordon, Synthesis, secondary structure and folding of the bend region of lung surfactant protein B, Pept. Res. 9 (1996) 28–39.
[10] P. Cai, C. Flach, R. Mendelsohn, An infrared reflection-absorption spectroscopy study of the secondary structure in (KL4)4K, a therapeutic agent for respiratory distress syndrome, in aqueous monolayers with phospholipids, Biochemistry 42 (2003) 9446–9452.
[11] T.E. Wiswell, G.R. Knight, N.N. Finer, S.M. Donn, H. Desai, W.F. Walsh, K.C. Sekar, G. Bernstein, M. Keszler, V.E. Visser, et al., A multicenter, randomized, controlled trial comparing Surfaxin (Lucinactant) lavage with standard care for treatment of meconium aspiration syndrome, Pediatrics 109 (2002) 1081–1087.
[12] V. Booth, A.J. Waring, F.J. Walther, K.M.W. Keough, NMR structures of the C-terminal segment of surfactant protein B in detergent micelles and hexafluoroisoporopanol, Biochem. (2004) (in press).
[13] M.L. Longo, A.M. Bisagno, J.A. Zasadzinski, R. Bruni, A.J. Waring, A function of lung surfactant protein SP-B, Science 261 (1993) 453–456.
[14] M.M. Lipp, K.Y.C. Lee, J.A. Zasadzinski, A.J. Waring, Phase and morphology changes in lipid monolayers induced by SP-B protein and its amino-terminal peptide, Science 273 (1996) 1196–1199.
[15] B. Fan, R. Bruni, W. Taeusch, R. Findlay, A. Waring, Antibodies against synthetic amphipathic helical sequences of surfactant protein SP-B detect a conformational change in the native protein, FEBS Lett. 282 (1991) 220–224.
[16] E.J.A. Veldhuizen, A.J. Waring, F.J. Walther, J.J. Batenburg, L.M.G. van Golde, H.P. Haagsman, Dimeric N-terminal segment of human surfactant protein B (dSP-$B_{1–25}$) has enhanced surface properties compared to monomeric SP-$B_{1–25}$, Biophys. J. 79 (2000) 377–384.
[17] M.M. Lipp, K.Y.C. Lee, D.Y. Takamoto, J.A.N. Zasadzinski, A.J. Waring, Coexistence of buckled and flat monolayers, Phys. Rev. Lett. 81 (1998) 1650–1653.
[18] R.V. Diemel, M.M.E. Snel, A.J. Waring, F.J. Walther, L.M.G. van Golde, G. Putz, H.P. Haagsman, J.J. Batenburg, Multilayer formation upon compression of surfactant monolayers depends on protein concentration as well as lipid composition: an atomic force microscopy study, J. Biol. Chem. 277 (2002) 21179–21188.
[19] J. Ding, I. Doudevski, H.E. Warriner, T. Alig, J.A.N. Zasadzinski, A.J. Waring, M.A. Sherman, Nanostructure changes in lung surfactant monolayers induced by interactions between palmitoyloleoylphosphatidylglycerol and surfactant protein B, Langmuir 19 (2003) 1539–1550.
[20] A. Waring, W. Taeusch, R. Bruni, J. Amikhanian, B. Fan, R. Stevens, J. Young, Synthetic amphipathic sequences of surfactant protein-B mimic several physiochemical and in-vivo properties of native pulmonary surfactant proteins, Pept. Res. 2 (1989) 308–312.
[21] M. Gupta, J. Hernandez-Juviel, A.J. Waring, F.J. Walther, Function and inhibition sensitivity of the N-terminal segment of surfactant protein B (SP-$B_{1–25}$) in preterm rabbits, Thorax 56 (2001) 871–876.
[22] F.J. Walther, J. Hernandez-Juviel, P.E. Mercado, L.M. Gordon, A.J. Waring, Surfactant with SP-B and SP-C analogues improves lung function in surfactant-deficient rats, Biol. Neonate 82 (2002) 181–187.
[23] K.Y. Lee, J. Majewski, T.L. Kuhl, P.B. Howes, K. Kjaer, M.M. Lipp, A.J. Waring, J.A.N. Zasadzinski, G.S. Smith, Synchrotron X-ray study of lung surfactant-specific protein SP-B in lipid monolayers, Biophys. J. 81 (2001) 572–585.
[24] B.N. Flanders, S.A. Vickery, R.C. Dunn, Imaging of monolayers composed of palmitic acid and lung surfactant protein B, J. Microsc. 202 (2001) 379–385.
[25] Y.N. Kaznessis, S. Kim, R.G. Larson, Specific mode of interaction between components of model pulmonary surfactants using computer simulations, J. Mol. Biol. 322 (2002) 569–582.
[26] J.A. Freites, Y. Choi, D.J. Tobias, Molecular dynamics simulations of a pulmonary surfactant protein B peptide in a lipid monolayer, Biophys. J. 84 (2003) 2169–2180.
[27] C.G. Fields, D.H. Lloyd, R.L. Macdonald, K.M. Ottenson, R.L. Noble, HBTU activation for automated Fmoc solid-phase peptide synthesis, Pept. Res. 4 (1991) 95–101.

[28] L.M. Gordon, S. Horvath, M.L. Longo, J.A.N. Zasadzinski, H.W. Taeusch, K. Faull, C. Leung, A.J. Waring, Conformation and molecular topography of the N-terminal segment of surfactant protein-B in structure-promoting environments, Prot. Sci. 5 (1996) 1662–1675.
[29] A.D. Williams, J.M. Wilkin, R.A. Dluhy, An investigation of miscibility in monolayer films of phosphocholine–phosphoglycerol binary mixtures, Colloids Surf. A 102 (1995) 231–245.
[30] P. Krüger, M. Schalke, Z. Wang, R.H. Notter, R.A. Dluhy, M. Lösche, Effect of hydrophobic surfactant peptides SP-B and SP-C on binary phospholipid monolayers: I. Fluorescence and dark-field microscopy, Biophys. J. 77 (1999) 903–914.
[31] P. Krüger, J.E. Baatz, R.A. Dluhy, M. Lösche, Effect of the hydrophobic peptide SP-C on binary phospholipid monolayers. Molecular machinery at the air/water interface, Biophys. Chem. 99 (2002) 209–228.
[32] K. Nag, J. Perez-Gil, A. Cruz, K.M.W. Keough, Fluorescently labeled pulmonary surfactant protein C in spread phospholipid monolayers, Biophys. J. 71 (1996) 246–256.
[33] K. Nag, S.G. Taneva, J. Perez-Gil, A. Cruz, K.M.W. Keough, Combinations of fluorescently labeled pulmonary surfactant proteins SP-B and SP-C in phospholipid films, Biophys. J. 72 (1997) 2638–2650.
[34] K. Nag, K.M.W. Keough, Epifluorescence microscopic studies of monolayers containing mixtures of dioleoyl- and dipalmitoylphosphatidylcholines, Biophys. J. 65 (1993) 1019–1026.
[35] B.M. Discher, K.M. Maloney, J.W.R. Schief, D.W. Grainger, V. Vogel, S.B. Hall, Lateral phase separation in interfacial films of pulmonary surfactant, Biophys. J. 71 (1996) 2583–2590.
[36] B.M. Discher, W.R. Schief, V. Vogel, S.B. Hall, Phase separation in monolayers of pulmonary surfactant phospholipids at the air-water interface: composition and structure, Biophys. J. 77 (1999) 2051–2061.
[37] A. Gopal, K.Y.C. Lee, Morphology and collapse transitions in binary phospholipid monolayers, J. Phys. Chem. B 105 (2001) 10348–10354.
[38] P. Krüger, M. Lösche, Molecular chirality and the domain shapes in lipid monolayers on aqueous surfaces, Phys. Rev. E. 62 (2000) 7031–7043.
[39] D. Dieudonne, R. Mendelsohn, R.S. Farid, C. Flach, Secondary structure in lung surfactant SP-B peptides: IR and CD studies of bulk and monolayer phases, Biochem. Biophys. Acta 1511 (2001) 99–112.
[40] Y.D. Wang, K.M.K. Rao, E. Demchuk, Topographical organization of the N-terminal segment of lung pulmonary surfactant protein B ($SP\text{-}B_{1-25}$) in phospholipid bilayers, Biochemistry 42 (2003) 4015–4027.
[41] F. Bringezu, J.Q. Ding, G. Brezesinski, A.J. Waring, J.A. Zasadzinski, Influence of pulmonary surfactant protein B on model lung surfactant monolayers, Langmuir 18 (2002) 2319–2325.